Scapholunate kinematics after flexible anchor repair

François Loisel, Stan Durand, Sylvain Persohn, Sébastien Aubry, Daniel Lepage, Xavier Bonnet, Wafa Skalli

Scapholunate kinematics after flexible anchor repair

François Loisel[a, b, *], Stan Durand[a], Sylvain Persohn[a], Sébastien Aubry[c], Daniel Lepage[b], Xavier Bonnet[a], Wafa Skalli[a]

[a] ENSAM, Institut de Biomécanique Humaine G. Charpark, 151, Boulevard de l'Hôpital, 75013 Paris, France
[b] Service de Chirurgie Orthopédique, Traumatologique, Plastique et Reconstructrice, SOS Main, CHU J. Minjoz, 3 Bd A. Fleming, 25000 Besançon, France
[c] Service de Radiologie Ostéoarticulaire, CHU J. Minjoz, 3 Bd A. Fleming, 25000 Besançon, France

Keywords:
Kinematics
Scapholunate ligament
Flexible anchors
Biplane X-ray

A B S T R A C T

The scapholunate joint is one of the keystones of the wrist kinematics, and its study is difficult due to the carpal bones size and the richness of surrounding ligaments. We propose a new method of quantitative assessment of scapholunate kinematics through bone motion tracking in order to investigate scapholunate ligament lesion as well as repair techniques. On 6 intact wrists, steel beads were inserted into the bones of interest to track their motions. Experimental set up allowed wrist flexion extension and radio-ulnar deviation motions. Low-dose bi-planar radiographs were performed each 10° of movement for different configurations: 1) intact wrist, 2) scapholunate ligament division, 3) repair by soft anchors at the posterior then 4) anterior part. Beads' 3D coordinates were computed at each position from biplanar X-Rays, allowing accurate registration of each wrist bone. The Monte Carlo sensitivity study showed accuracy between 0.2° and 1.6 ° for the scaphoid and the lunate in motions studied. The maximum flexion-extension range of motion of the scaphoid significantly decreased after anterior repair from 73° in injured wrist to 62.7°.

The proposed protocol appears robust, and the tracking allowed to quantify the anchor's influence on the wrist kinematics.

1. Introduction

The wrist can be schematized into a dual linkage system including the proximal and the distal carpal row, in which each bone in a given row moves in the same direction during wrist motion. The scapholunate interosseus ligament (SLIL) is a complex anatomical structure connecting the scaphoid to the lunate within the first row of carpal bones. Therefore, during wrist flexion or radial deviation, the distal part of the scaphoid flexes which leads lunate into flexion through the SLIL. This ligament is also critical for complex wrist movements useful in daily living functions, such as the dart throwing motion. When this ligament is completely torn and the scapholunate joint becomes dissociated, the dorsal and lateral aspect of radioscaphoid fossa becomes stressed because the forces crossing the wrist cannot be distributed normally.

Sooner or later, this instability leads to a predictable course of degenerative arthritis called scapho-lunate advanced collapse (SLAC).

Although the dorsal component of the SLIL is widely considered as the most resilient [1,2], recent work highlighted that the loads to failure between dorsal and volar part of the ligament are not statistically different [2].

From a mechanical perspective, the aim of a surgical repair or ligamentoplasty is the substitution of the SLIL using biomaterials (bone-ligament-bone autografts or other solution [3–6]) allowing wrist motions recovery and physiological load distribution.

The study of scapholunate joint kinematics is challenging because the carpal bones are small and the surrounding ligament structures are complex.

There are only few studies investigating the effect of the surgery for the restoration of the scapholunate kinematics [7,8].

Those previous studies are based on different motion tracking methods making any comparison difficult. For example, two studies [9,10] computed their geometrical parameters such as the

* Corresponding author at: Service de chirurgie Orthopédique, Traumatologique, Plastique et Reconstructrice, SOS Main, CHU J. Minjoz, 3 Bd A. Fleming, 25000 Besançon, France.
E-mail addresses: francois.loisel@gmail.com (F. Loisel), stan.durand@ensam.eu (S. Durand), sylvain.persohn@ensam.eu (S. Persohn), saubry@chu-besancon.fr (S. Aubry), dlepage@chu-besancon.fr (D. Lepage), xavier.bonnet@ensam.eu (X. Bonnet), wafa.skalli@ensam.eu (W. Skalli).

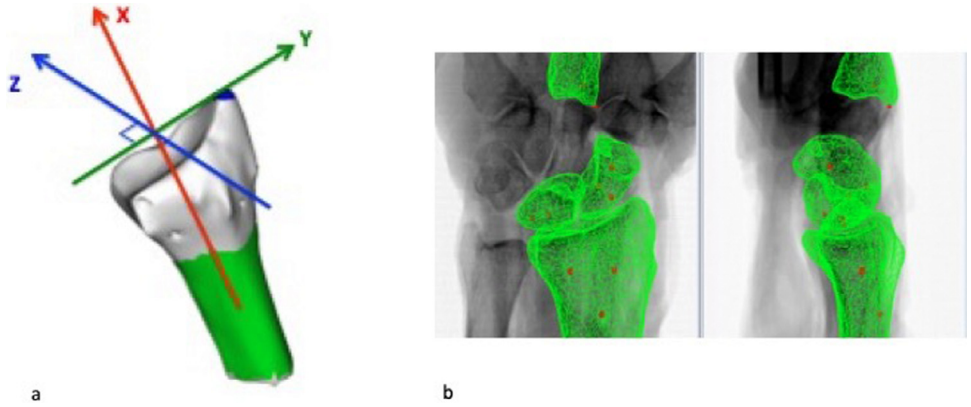

Fig. 1. a) Radius local frame: red axis = prono supination axis, green axis = Flexion Extension axis, blue axis = Radio Ulnar Deviation axis. A cylinder is fitted with a least square condition to the green area to obtain the prono supination axis and the radius styloid is manually selected and corresponds to the barycenter of the blue area. b) Registration of the three bones considered using the bead 3D coordinates (in red the beads). (For interpretation of the references to color in this figure legend, the reader is referred to the web version of this article.)

gap between the lunate and the scaphoid using a single 2D X-ray posteroanterior (PA) radiograph of the wrist, which means that their results may be affected by the projection of 3D shapes onto a 2D plane compared to other studies measuring the same distance in 3D using biplanar radiographs [7] or electromagnetic (EM) sensors [8].

In addition, one could question the impact of the EM sensors on the wrist kinematics.

Recent approaches use biplanar X-Rays with embedded radiopaque markers for bone tracking [11–13].

Thus, we propose a new method of quantitative assessment of scapholunate kinematics through bone motion tracking allowing the investigation of scapho-lunate ligament lesion as well as techniques of repair. The objectives of this study are two-fold: the evaluation of the accuracy of this new method and the analysis of the effect of the modelization of an additional volar repair of the scapho-lunate ligament.

2. Methods

2.1. Dissection and inclusion of the wrists

Six arms from 3 female cadavers were collected from the anatomy laboratory of our university hospital in a frozen state and subsequently thawed at room temperature.

Wrist arthroscopy were performed to check the integrity of the SLIL: we classified the scapho-lunate joint instability according to the Geissler and the European Wrist Arthroscopy Society (EWAS) classification [14,15] (wrists having a scapho-lunate joint state smaller than 2 are considered to be stable).

The morphology of the lunate was classified according to Viegas [16]. All the anatomical structures have been preserved. A longitudinal dorsal and palmar incision from the entire forearm to the base of the third finger as well as retinaculum of the flexors and extensors was performed to allow access to the joint capsule. The set of epidemiological characteristics of the wrists are summarized in Table 1.

2.2. Setting up markers

Steel beads were introduced under fluoroscopic control (Siemens Siremobil Compact, Siemens AG, Munich, Germany) three by three, within the lunate, the base of the third metacarpal (1 mm beads). the scaphoid and the distal radius epiphysis (1.5 mm beads). These beads were placed manually after making a bone orifice using a Kirchner wire of diameter 1.2 and 1.6 respectively.

Table 1
Epidemiological characteristics of anatomical parts.

Age	Side	Arthroscopic assessment		Viegas classification
		Geissler	EWAS	
91	R	**I**	**1**	**2**
	L	**I**	**2**	**2**
89	R	**I**	**2**	**1**
	L	**I**	**2**	**1**
80	R	**II**	**2**	**1**
	L	**II**	**2**	**1**

Because wrist bones are very small, the robustness of each local frame was investigated as defined in Section 2.4.

2.3. Imaging and 3D modeling

Each included wrist was scanned with a bone density phantom using a Philips Brilliance 64 scanner (120 kV, 500 mA, Thornton, CO, USA), 0.5 mm thick, allowing for an accurate 3D reconstruction of wrist bones and steel beads using MITK software. Radius CT reconstruction allowed to define the wrist Flexion-Extension (FE), Radio-Ulnar Deviation (RUD), and Prono-Supination (PS) axes as described in the literature [17] (Fig. 1a). *X*-axis was defined as the axis of the best fit cylinder defined from the radius diaphysis. The *Y*-axis corresponded to the axis crossing the radius styloid secant and perpendicular to the *X*-axis. *Z* axis was defined by the cross product.

2.4. Kinematics analysis and experimental set up

Bone tracking was performed using low dose biplanar X-rays allowing the computation of the beads 3D coordinates. First, each segmented bone was positioned onto the first X rays acquisition using a rigid registration. Then, the bead positions at each wrist position were carefully checked. Since any bead sliding within the bone was not measured, for each step, the position of the bone was readjusted by rigid registration using the new beads 3D coordinates.

Custom software (Fig. 1b) was used to automatically record the beads 3D coordinates at each step, and custom MATLAB (Natick, USA) routines were used to compute the new position of each bone.

Given the small size of the bones, a Monte Carlo sensitivity study was performed to quantify the robustness of each local frame. A Gaussian noise with a range of motion (RoM) of 0.1 mm

Fig. 2. Test bench. Legend: the asterisk (*) represents the 3D printed base fixed to the reference plane. The crosses (+), the pulleys guiding the cables with 500 g masses (red arrow). The white arrow indicates the plate on which are fixed the fingers and the palm with the aid of a clamp. An intermediate piece connects it to the motor.

was applied to the bead coordinates using the MATLAB function randn. 500 "noisy" frames were compared to the initial frame to quantify the angular deviation induced by the noise. The standard deviation (1SD) of the angular deviation over the 500 iterations allowed us to estimate the reliability of each local frame.

The radius and third metacarpal positions were used to compute the wrist motion. From the radius local frame, scaphoid and lunate rotations and translations along wrist FE, RUD and PS in each wrist position were computed.

Based on morphometric data provided by the 3D reconstruction, the dimensions of the test bench could be adjusted for each specimen. The test bench consisted of a 3D printed base attached to the reference plane. In this base, the forearm was positioned in a neutral prono-supination position by two 35 mm screws and fixed by a PMMA surgical cement. All the wrist and finger tendons were secured in three groups at the volar and the posterior part of the wrist to which a force of 5 N was transmitted through pulleys (Fig. 2).

The hand was fixated to a perforated plate using straps around each finger and the wrist to remove any sliding effect during the imposed motion.

The hand motion was controlled in displacement. The test bench was specifically designed to impose pure planar motions.

The RoMs considered are FE (y-axis) ranging from 30° flexion to 60° extension, and RUD (z-axis) from 20° radial deviation to 30° ulnar deviation.

Table 2
Monte Carlo sensivity study (1 SD, degrees) for each bone according the 3 axes.

	Lunate	Scaphoid	3rd metacarpal
X axis (Pronation – Supination)	1.4	3.0	1.0
Y axis (Flexion - Extension)	1.5	0.2	1.0
Z axis (Radial - Ulnar deviation)	1.6	0.2	1.0

An EOS biplanar X-Rays acquisition (EOS imaging, Paris, France) was performed every 10° after performing a cycling test of 5 cycles.

For each wrist, movements were performed when the wrist was intact, after SLIL lesion, dorsal repair and both dorsal and volar repair.

Injury and repairs were performed by a senior hand surgeon.

Injury consisted in sectioning the dorsal and the volar parts of the SLIL as well as the dorsal radiocarpal ligament (DRC) and dorsal intercarpal ligament (DIC) with a blade.

Finally, the modelling of the ligament was performed using 1 mm soft anchors (Juggerknot, ZimmerBiomet, Warsaw, USA) (Fig. 3). For the third configuration: one anchor was inserted at the posterior and proximal part of the scaphoid and another one parallel in the lunate. The threads of the two anchors were knotted together with a Nicky's knot. For the last configuration, an additional volar repair was modelized by the same procedure at the anterior part of the scaphoid and the lunate.

2.6. Statistics

For each subject, the kinematics has been studied on the intact wrist injured, after repair of the dorsal part of the ligament and finally after further repair of the anterior part of the ligament. Friedman's statistical tests were generated, and a Wilcoxon test was performed for the significative values as a *post-hoc* study using SPSS Statistics® software for Mac (Version 25, SPSS, IBM, NY, USA).

The threshold of significance was $P < 0.05$.

3. Results

The results of the sensitivity study have shown a measurement accuracy between 0.2° and 1.6° concerning the motions of interest (FE and RUD) (Table 2). There was a significant difference within the different configurations during FE of the wrist for the FE of the scaphoid ($p = 0.03$), and the translation along the RUD axis ($p = 0.01$). During RUD of the wrist, there were also significant differences for the RUD of the scaphoid ($p = 0.01$) and the translation along the FE axis ($p = 0.003$) and the RUD axis ($p = 0.02$). There were no significant changes for the lunate motions during FE or RUD of the wrists. All the results of the RoM of the scaphoid and the lunate concerning the configuration and the direction of the displacement of the wrist are presented in the annex.

The *post-hoc* study that focused on the rotation of the scaphoid around the Y-axis during FE of the wrist (Fig. 4a) has shown a significant increase of the motion of the scaphoid between the intact configuration and the injured one (63.8° to 73°) and a significant decrease between the injured and the additionnal volar repair configuration (73° to 62.7°). For the Z-axis, during RUD of the wrist (Fig. 4b), we found the same behavior (29.3° to 33.3° and 33.3° to 30.7°, respectively). For the scaphoid/lunate translation along Z-axis, for the FE of the wrist (Fig. 5a) or along Y-axis for RUD of the wrist (Fig. 5b), the results have shown a significant difference between the intact and the injured wrist (1.9 mm to 4.1 mm, and 1.1 mm to 2.8 mm) but no differences among the two repair modalities.

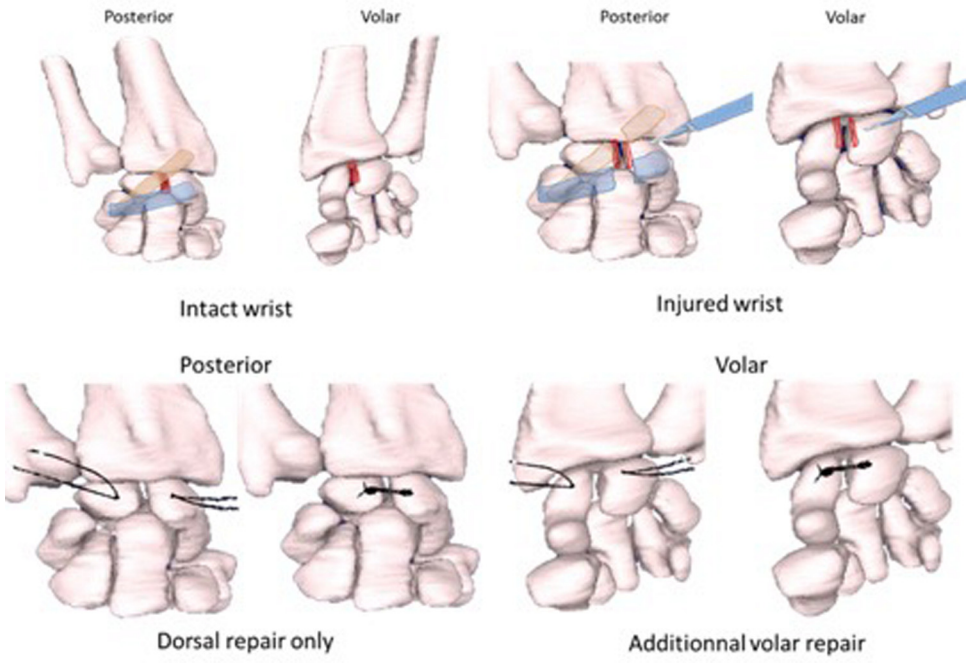

Fig. 3. Ligament injuries and repairs. Legend: Intact configuration: Dorsal Radio Carpal (DRC) ligament in orange, Dorsal Intercarpal (DIC) ligament in blue, posterior and volar part of the SLIL in red. Injured configuration: realization of the lesion of the DRC, DIC and the posterior and the volar part of the SLIL. "Dorsal repair only" configuration: placement of anchors at posterior part of the scaphoid and the lunate and fixed together. Additional volar repair configuration: same additional procedure on the volar part of these bones.

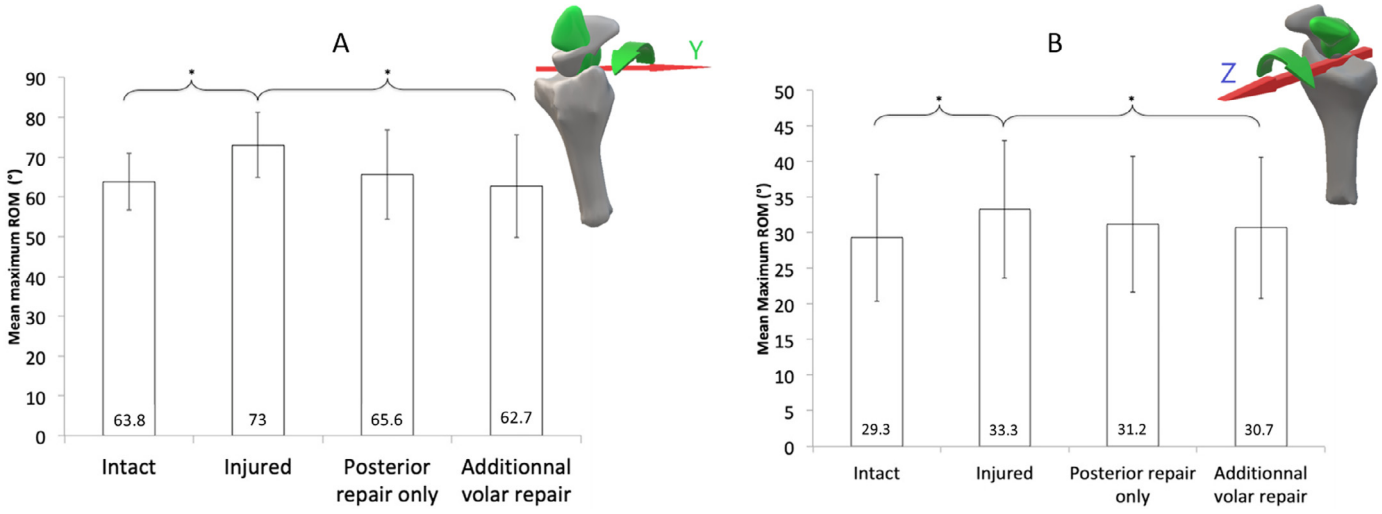

Fig. 4. a) Mean maximum RoM of the rotation (°) of the scaphoid around the *Y-axis* during FE of the wrist for the four configurations.
b) Mean maximum RoM of the rotation (°) of the scaphoid around the *Z*-axis during RUD of the wrist for the four configurations. * correspond to $P < 0.5$.

4. Discussion

Quantitative assessment of physiological kinematics, the effect of a potential lesion or even surgical restoration is difficult with respect to this joint due to the uncertainty of tracking wrist bone movements.Our original approach was to perform the analysis of the scapholunate kinematics in vitro using a low dose biplane x-ray with intraosseous markers tracking the bone. Furthermore, different configurations of the wrist were compared: when the SLIL was intact, then divided and repaired by soft anchors.

A significant increase of the RoM of the scaphoid between intact and injured configurations along FE (during FE of the wrist) and RUD (during RUD of the wrist) was observed.

The modeling of an additional volar repair significantly decreased the RoM.

The reported trends concerning the scaphoid RoM before and after the lesion are consistent with the literature. In particular, Waters et al. [18] highlighted the same increase in scaphoid flexion in injured wrists.

Regarding the lunate, while the literature reported that SLIL lesion increases lunate extension from 5.4° to 15°, we found a greater variability ranging from 11.8° in extension to 7.4° in flexion (Table 3).

The wide range of RoM reported in the literature [19,20] underlines the multiple challenges of this type of investigation such as great inter-individual variations or the reproducibility of the ligamentous lesion [18].

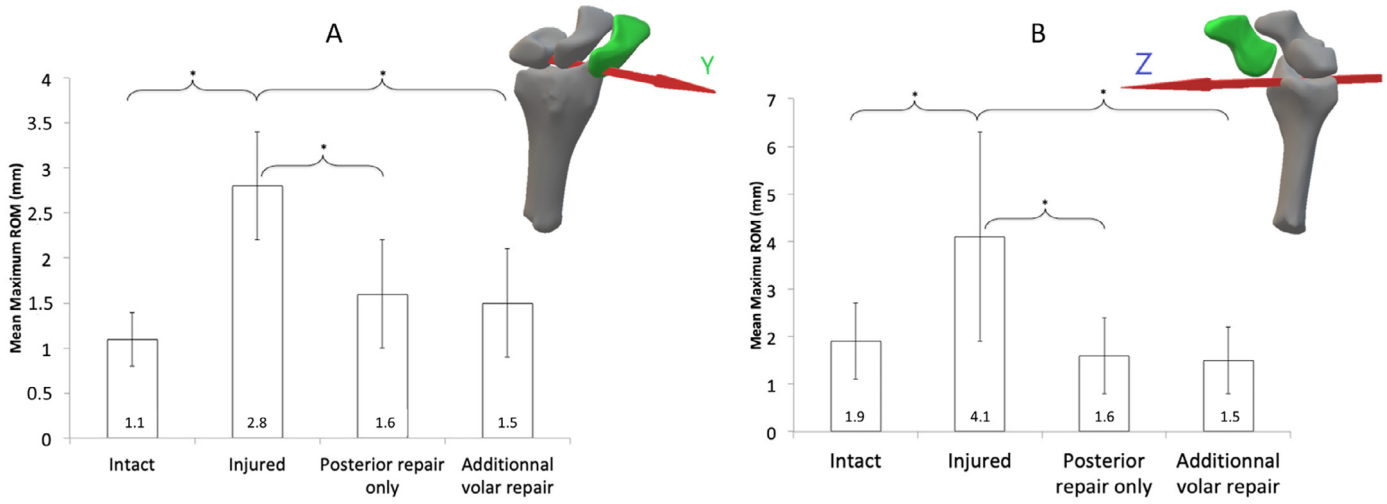

Fig. 5. a) Mean maximum RoM of the translation (mm) of the scaphoid/lunatum along the *Z*-axis during FE of the wrist for the four configurations.
b) Mean maximum RoM of the translation (mm) of the scaphoid/lunatum along the *Y*-axis during RUD of the wrist for the four configurations. * correspond to $P < 0.5$.

Table 3
Comparative study of the literature comparing FE RoMs of the scaphoid and lunate before and after ligament injury in FE of the wrist. SLIL = Scapho Lunate Inter osseus Ligament, ST = Scapho Trapezial Ligaments, RSC = Radio Scapho Capitate Ligament, DRC = Dorsal Radio Carpal Ligament, DIC = Dorsal Inter Carpal Ligament, EM= ElectroMagnetic sensors. + = flexion; - = extension.

Autors, year	Number of wrists	Method	Lesion(s)/ Repair	Kinematics (°)	FE Scaphoide effect of the lesion (°)	FE Lunate effect of the lesion (°)
Short, 1995 [21]	6	EM sensors/ active wrist simulator	SLIL	FE: 50–30	+ 3.6	- 5.4
Short, 2002 [22]	8	EM sensors/ active wrist simulator	SLIL + ST + RSC	FE: 40–30	+	–
Short, 2005 [23]	24	EM sensors/ active wrist simulator	SLIL + ST + RSC	FE: 50–30	+ >2	- >2
Short, 2007 [24]	24	EM sensors/ active wrist simulator	SLIL + DRC + DIC	FE: 50–30	+ 3.9	- 6.4
Short, 2009 [8]	8	EM sensors/ active wrist simulator	SLIL + DRC + DIC	FE: 50–30	+	–
Stilling, 2010 [20]	12	tantalum beads, preformed plate, biplanar radiographs	ST	0 /E 30	+	Not studied
Eschweiler, 2016 [26]	8	EM sensors/ passive wrist simulator	SLIL	FE: 30–30	+ 2	No difference [<1]
Waters, 2016 [18]	16	EM sensors/ active wrist simulator	SLIL	FE: 50–30	+ 9	- 15
Current Study, 2018	6	wrists, passive wrist simulator	SLIL + DIC + DRC	FE: 30–60	**+ 9.2 [6.5 - 12.5]**	**+ 2.9 [–11.8 - 7.4]**

From Table 3, it is noticeable that most of the previous studies [8,18,21–26] used an active motion simulator coupled with EM sensors.

Although active motion simulators allow to produce hand motions closer to the physiological behavior by stretching the tendons which helps to emulate wrist rotations, the use of EM sensors fixated to the dorsal face of the wrist by means of carbon rod could interfere with the joint kinematics by exerting non-physiological forces onto the soft tissues. In addition, the use of EM sensors induces an asymmetric RoM more important in flexion (50°) than in extension (30°) due to the presence of the sensors on the dorsal side.

Our work is interested in studying the effect of a surgical treatment on scapholunate kinematics, which unfortunately is not well documented in the literature [7,8].

Slater et al. [7] have shown that the lesion increases the gap between scaphoid and lunate in clenched fist position (2.1 mm in intact versus 8 mm in injured wrist) and the repair decreased the diastasis: between 3.1 mm and 5.8 mm according to the type of capsulodesis.

Similarly, Pollock et al. [9] highlighted an increase in the scapho-lunate gap from 2.9 mm when the ligaments are intact to 5.0 mm when the ligaments are sectioned. The repair decreased the pathological gap from 2.6 mm to 4.6 mm according to the type of capsulodesis.

Although a similar increase was observed, the lower values reported in this paper, around 1 mm for the intact configuration and about 3 mm for the injured one, are most likely due to the wrist configuration (passive RoM versus clenched fist position).

From our results, although the lunate seems less affected, the volar repair of the ligament tends to improve the scaphoid kinematics and reduce the distance between the scaphoid and the lunate. Thus, this study suggests that a combined posterior and anterior repair may be helpful in improving scapholunate kinematics after injury.

Based on the Monte Carlo sensitivity study, uncertainty of the carpal bone displacements was quantified, with values ranging from 0.2° to 1.6° concerning the FE and the RUD axis. The scaphoid and lunate frames were more sensitive to the bead displacements because the beads were closer to each other compared to the beads inside the radius or the third metacarpal. While the results were all processed, the analysis focused on rotations in the *Y* and *Z*-axis corresponding to the displacement imposed by the motor. Indeed, for the scaphoid, the estimated uncertainty along the *Z*-axis was relatively high (3°). This uncertainty could be reduced by positioning the beads further away from each other. Nevertheless, although the carpal bones are very small, we managed to get robust local frames as well as preserving the ligament integrity. In addition, the reported changes in scaphoid and lunate RoM along wrist FE and RUD after injury and ligament repair are both higher than the uncertainty, and consistent with the literature.

Our study has some limitations: the relative low number of wrists and the use of a passive wrist movement simulator which

does not consider the transmission of forces within the joint produced by an active contraction of the wrist tendons.

Despite these limitations, the proposed protocol has several major strong points: minimally invasive intraosseous radio-opaque makers that both preserve the integrity of ligaments and prevent from extrinsic sensor limitations. The integrity of the SLIL examined in situ under prior arthroscopy is also a pledge of rigor because the proportion of ligamentous lesions on the cadaveric is significant: 43% in our study, ranging from 16% to 50% in the literature [27–29].

This preliminary study seeks to accuratly understand the scapholunate kinematics. Our results about the wrist kinematics are consistent with previously reported values. The scapholunate kinematics analysis highlights how the lesion alters the bone motions and how the anchors tend to restore the physiological kinematics. Further investigation on larger samples would be highly valuable to track subject-specific variabilities and strengthen the trends reported in this paper. Our protocol can also be easily extended to other wrist bones to investigate the impact of the lesion at a larger scale within the wrist.

Declaration of Competing Interest

Non-financial support from ZimmerBiomet, non-financial support from Stryker, non-financial support from Arthrex, financial support from FH orthopedics (travel fellowship grant) outside the submitted work.

Aknowledgement

Dr Quentin Lepiller for the virological analysis of the cadaveric parts, Pr. Tatu and Pr. Parratte for the provision of cadaveric specimen, Hugues Grandin, Emmanuel Laurent and Martial Bulle for the technical help, Thomas Joubert for his technical support., David Jinseong Kim for his proofreading and English correction.

Funding

ZimmerBiomet, Biomecam Chair program on subject specific musculoskeletal modelling.

Ethical Approval

[1] Berger RA, Imeada T, Berglund L, An KN. Constraint and material properties of the subregions of the scapholunate interosseous ligament. J Hand Surg 1999;24:953–62.

[2] Nikolopoulos FV, Apergis EP, Poulilios AD, Papagelopoulos PJ, Zoubos AV, Kefalas VA. Biomechanical properties of the scapholunate ligament and the importance of its portions in the capitate intrusion injury. Clin Biomech Bristol Avon 2011;26:819–23.

[3] Hofstede DJ, Ritt MJ, Bos KE. Tarsal autografts for reconstruction of the scapholunate interosseous ligament: a biomechanical study. J Hand Surg 1999;24:968–76.

[4] Shin SS, Moore DC, McGovern RD, Weiss AP. Scapholunate ligament reconstruction using a bone-retinaculum-bone autograft: a biomechanic and histologic study. J Hand Surg 1998;23:216–21.

[5] Cuénod P, Charrière E, Papaloïzos MY. A mechanical comparison of bone-ligament-bone autografts from the wrist for replacement of the scapholunate ligament. J Hand Surg 2002;27:985–90.

[6] Ehsan A, Lee DG, Bakker AJ, Huang JI. Scapholunate ligament reconstruction using an acellular dermal matrix: a mechanical study. J Hand Surg 2012;37:1538–42.

[7] Slater RR, Szabo RM, Bay BK, Laubach J. Dorsal intercarpal ligament capsulodesis for scapholunate dissociation: biomechanical analysis in a cadaver model. J Hand Surg 1999;24:232–9.

[8] Short WH, Werner FW, Sutton LG. Dynamic biomechanical evaluation of the dorsal intercarpal ligament repair for scapholunate instability. J Hand Surg 2009;34:652–9.

[9] Pollock PJ, Sieg RN, Baechler MF, Scher D, Zimmerman NB, Dubin NH. Radiographic evaluation of the modified brunelli technique versus the blatt capsulodesis for scapholunate dissociation in a cadaver model. J Hand Surg 2010;35:1589–98.

[10] Lee SK, Zlotolow DA, Sapienza A, Karia R, Yao J. Biomechanical comparison of 3 methods of scapholunate ligament reconstruction. J Hand Surg 2014;39:643–50.

[11] Tsai T-Y, Dimitriou D, Hosseini A, Liow MHL, Torriani M, Li G, et al. Assessment of accuracy and precision of 3D reconstruction of unicompartmental knee arthroplasty in upright position using biplanar radiography. Med Eng Phys 2016;38:633–8.

[12] Fayyazi AH, Ordway NR, Park S-A, Fredrickson BE, Yonemura K, Yuan HA. Radiostereometric analysis of postoperative motion after application of dynesys dynamic posterior stabilization system for treatment of degenerative spondylolisthesis. J Spinal Disord Tech 2010;23:236–41.

[13] Garner MR, Dow M, Bixby E, Mintz DN, Widmann RF, Dodwell ER. Evaluating length: the use of low-dose biplanar radiography (EOS) and tantalum bead implantation. J Pediatr Orthop 2016;36:e6–9.

[14] Geissler WB, Freeland AE, Savoie FH, McIntyre LW, Whipple TL. Intracarpal soft-tissue lesions associated with an intra-articular fracture of the distal end of the radius. J Bone Joint Surg Am 1996;78:357–65.

[15] Messina JC, Van Overstraeten L, Luchetti R, Fairplay T, Mathoulin CL. The ewas classification of scapholunate tears: an anatomical arthroscopic study. J Wrist Surg 2013;2:105–9.

[16] Viegas SF, Wagner K, Patterson R, Peterson P. Medial (hamate) facet of the lunate. J Hand Surg 1990;15:564–71.

[17] Wu G, van der Helm FCT, Veeger HEJD, Makhsous M, Van Roy P, Anglin C, et al. ISB recommendation on definitions of joint coordinate systems of various joints for the reporting of human joint motion–Part II: shoulder, elbow, wrist and hand. J Biomech 2005;38:981–92.

[18] Waters MS, Werner FW, Haddad SF, McGrattan ML, Short WH. Biomechanical evaluation of scaphoid and lunate kinematics following selective sectioning of portions of the scapholunate interosseous ligament. J Hand Surg 2016;41:208–13.

[19] Stromps JP, Eschweiler J, Knobe M, Rennekampff HO, Radermacher K, Pallua N. Impact of scapholunate dissociation on human wrist kinematics. J Hand Surg Eur Vol 2018;43:179–86.

[20] Stilling M, Krøner K, Rømer L, Van De Giessen M, Munk B. Scaphoid kinematics before and after scaphotrapeziotrapezoidal ligament section. Assessment by radiostereometric analysis and computed tomography in a cadaver study. J Hand Surg Eur Vol. 2010;35:637–45.

[21] Short WH, Werner FW, Fortino MD, Palmer AK, Mann KA. A dynamic biomechanical study of scapholunate ligament sectioning. J Hand Surg 1995;20:986–99.

[22] Short WH, Werner FW, Green JK, Masaoka S. Biomechanical evaluation of ligamentous stabilizers of the scaphoid and lunate. J Hand Surg 2002;27:991–1002.

[23] Short WH, Werner FW, Green JK, Masaoka S. Biomechanical evaluation of the ligamentous stabilizers of the scaphoid and lunate: part II. J Hand Surg 2005;30:24–34.

[24] Short WH, Werner FW, Green JK, Sutton LG, Brutus JP. Biomechanical evaluation of the ligamentous stabilizers of the scaphoid and lunate: part III. J Hand Surg 2007;32:297–309.

[25] Werner FW, Sutton LG, Allison MA, Gilula LA, Short WH, Wollstein R. Scaphoid and lunate translation in the intact wrist and following ligament resection: a cadaver study. J Hand Surg 2011;36:291–8.

[26] Eschweiler J, Stromps JP, Rath B, Pallua N, Radermacher K. Analysis of wrist bone motion before and after SL-ligament resection. Biomed Tech 2016;61:345–57.

[27] Viegas SF, Yamaguchi S, Boyd NL, Patterson RM. The dorsal ligaments of the wrist: anatomy, mechanical properties, and function. J Hand Surg 1999;24:456–68.

[28] Overstraeten LV, Camus EJ, Wahegaonkar A, Messina J, Tandara AA, Binder AC, et al. Anatomical description of the dorsal capsulo-scapholunate septum (DCSS)-arthroscopic staging of scapholunate instability after DCSS sectioning. J Wrist Surg 2013;2:149–54.

[29] Loisel F, Cohen G, Marès O, Garret J, Clavert P. Kystes mucoïdes de la face dorsale du poignet : lésions anatomiques, place de la prise en charge chirurgicale et technique opératoire. Rev Chir Orthopédique Traumatol 2017;103:S185–92.